Biosensors and Bioelectronics 102 (2018) 321–327

Contents lists available at ScienceDirect

Biosensors and Bioelectronics

journal homepage: www.elsevier.com/locate/bios

Sandwich-type biosensor for the detection of α2,3-sialylated glycans based on fullerene-palladium-platinum alloy and 4-mercaptophenylboronic acid nanoparticle hybrids coupled with Au-methylene blue-MAL signal amplification

Qiqi Yuan[1], Junlin He[1], Yazhen Niu, Jun Chen, Yilin Zhao, Yuchan Zhang, Chao Yu*

College of Pharmacy, School of Public Health and Management, and Chongqing Pharmacodynamic Evaluation Engineering Technology Research Center, Chongqing Medical University, Chongqing 400016, PR China

ARTICLE INFO

Keywords:
Sandwich-type sensor
α2,3-sialylated glycans
4-mercaptophenylboronic acid
Maackia amurensis lectin
Methylene blue

ABSTRACT

α2,3-sialylated glycans (α2,3-sial-Gs) are one of the significant tumour biomarkers for the early diagnosis of cancer. In this work, a neoteric sandwich-type biosensor was developed for detecting α2,3-sial-Gs using 4-mercaptophenylboronic acid (4-MPBA) to construct a novel molecular recognition system by the coordination of a boron atom of 4-MPBA to the amide group of Neu5Ac in the α2,3-sial-Gs structure. Amino-functionalized fullerene coupled with palladium-platinum bimetallic alloy nanocrystals (n-C_{60}-PdPt) was synthesized to modify the surface of a glassy carbon electrode (GCE) because the n-C_{60} nanomaterial affords a large surface area for the on-site reduction of bimetallic alloy nanoparticles and an excellent capacity for electron transfer. Abundant 4-MPBA were immobilized on the n-C_{60}-PdPt, since the 4-MPBA has the mercapto group can combine with PdPt alloy through strong adsorption. Maackia amurensis lectin (MAL) was covalently immobilized on Au-poly (methylene blue) (Au-PMB) acting as the signal amplification components, which was used to recognize the α2, 3-sial-Gs specifically like a second antibody linked on Au-PMB. The differential pulse voltammetry (DPV) current response of the biosensor in 5 mL of PBS (0.1 M, pH = 7.4) was recorded, and the proposed sandwich-type biosensor showed a wide linear range of 10 fg mL^{-1} −100 ng mL^{-1} as well as, a low detection limit of 3 fg mL^{-1} (S/N = 3). Furthermore, the proposed method exhibited good recovery and stability, indicating its potential for use in clinical studies.

1. Introduction

N-acetylneuraminic acid (Neu5Ac, sialic acid) is attached to cell surface glycoconjugates as terminal monosaccharides, which are widely associated with biological function (Kim et al., 2011). The α2,3-linkage of sialic acid to N-acetyllactosamine structures (Galβ1-4GlcNAc) is formed by the enzyme β-galactoside α2,3-sialyltransferase (ST3Gal-I) (Harduin-Lepers et al., 2001; Park et al., 2012). Variants of α2,3-sialylation are relevant to the development of gastric cancer, pancreatic cancer, prostatic cancer (Chen and Varki, 2010; Leppanen et al., 2005; Park et al., 2012). When the apoptosis of carcinoma cells happens in tumour tissue, the α2, 3-sialylated glycans (α2,3-sial-Gs) are released into the blood, which results in an increase in the level of α2,3-sial-Gs in the blood of patients (Hsiao et al., 2016). In recent years, some efforts have been making to achieve the highly sensitive detection of α2, 3-sialylated glycan in human serum samples. (Everest-Dass et al., 2013; Patil et al., 2014; Kang et al., 2014; Niu et al., 2016; Palmisano et al., 2013). Therefore, finding and exploring a sensitive and specific detection methods of α2, 3-sial-Gs can contribute to the early diagnosis of cancer.

Up until now, only a few analytical methods have been applied to detect sialylated glycans, including electrospray mass spectrometry (MS) (Saarinen et al., 1999), tandem MS (Kang et al., 2014) and miniaturized glycosyltransferase assays (Patil et al., 2014). These methods have some advantages, such as good qualitative ability, the use of classic technology and high resolution. Nevertheless, they suffer from some common shortcomings such as a long analysis time as well as the need for high precision instrumentation and qualified personnel, which limit their widespread use (Kavosi et al., 2014). Thus, earlier attempts to explore novel detection techniques for the sensitive analysis of

* Correspondence to: College of Pharmacy, Chongqing Medical University, 1 Yi Xue Yuan Road, Box 380#, Chongqing 400016, PR China.
E-mail address: yuchaom@163.com (C. Yu).
[1] Junlin He and Qiqi Yuan contributed equally to this work.

https://doi.org/10.1016/j.bios.2017.11.043
Received 29 August 2017; Received in revised form 24 October 2017; Accepted 12 November 2017

cancer biomarkers, especially in the clinical applications, are highly significant. In recent years, sandwich-type biosensors are one of the important analytical techniques for the sensitive and specific detection of proteins (Feng et al., 2017; Xia et al., 2013). However, the use of this design to detect glycans is limited in biomedical applications because a second antibody against glycans could not be utilized in the methods.

The α2,3-sial-Gs, released from a α2,3-linkage of sialic acid to N-acetylactosamine structures in glycoconjugates, can usually be combined with specific lectins (Gao et al., 2014). Maackia amurensis lectin (MAL) is an ideal tool for the specific detection of α2,3-sial-Gs (Geisler and Jarvis, 2011) due to MAL combining specifically with the α2,3-sial-Gs structure. Therefore we selected MAL as one of specifically recognized components (Niu et al., 2016). To propose a sandwich-type electrochemical sensor, 4-mercaptophenylboronic acid (4-MPBA) was used as the capture molecule in the sensor for the first time. The formation of a trigonal-formed compound was stabilized by the coordination of a boron atom of 4-MPBA to the amide group of Neu5Ac, thus forming intramolecular B-O bonding (Otsuka et al., 2003). Therefore, a system based on MAL and 4-MPBA, which was employed as a novel recognition system for the detection of α2,3-sial-Gs, has been designed.

In this study, methylene blue (MB), the derivative of phenothiazine dye, was used for electrochemical redox-active species and as a signal material in the biosensors. However, it is difficult to produce a stable signal when MB is utilized alone. Therefore, we used Au nanoparticles to improve the stability of MB, due to their good electro-conductivity, large specific surface area, excellent biocompatibility and strong biological molecule absorbability (Zhang et al., 2013). Based on above-mentioned advantages, MAL immobilizes on the Au nanoparticles, and the signal amplification components can be built. MAL functionalized-poly(methylene blue) (MAL-Au-PMB) was facilely synthesized by the oxidative polymerization of MB and served as a novel redox species for the detection of α2,3-sial-Gs for the first time.

To achieve a highly sensitive sandwich-type biosensor, the synthesis of excellent materials to modify the electrode is important. In recent years, metal alloys, such as alloys of palladium and platinum (PdPt), have attracted remarkable attention (Chen et al., 2016) due to their high electrical conductivity, good stability and enlarged surface area (Li et al., 2014). We selected PdPt bimetallic alloy to be used to combine with the capture molecule in this study. To elevate the loading capacity of PdPt alloy on the glassy carbon electrode, amino-functionalized fullerene (n-C_{60}) was introduced. The n-C_{60} possessed a large surface area, outstanding electron acceptor capability (Li et al., 2013) and abundant amino groups for further modification. Accordingly, motivated by the advantages of the large loading capacity as well as the good conductivities of both the PdPt alloy and n-C_{60}, nano-composite materials were synthesized through stable conjunction between noble metal nanoparticles and amino groups. This allows more 4-MPBA (Zhang et al., 2004), as the capture molecule, to be fixed onto the n-C_{60}-PdPt nano-composite materials. In summary, the combination of n-C_{60}-PdPt and 4-MPBA achieved a specific detection platform for α2,3-sial-Gs.

Here, we report an ultrasensitive sandwich-type biosensor for the specific detection of α2,3-sial-Gs utilizing 4-MPBA@n-C_{60}-PdPt as the support platform and MAL-Au-PMB composites as the signal amplification tag. The synthetic method possesses greater practicality and repeatability. The spiked serum samples were detected. The proposed sandwich-type biosensor showed ultra-sensitivity, high precision, good stability, and good reproducibility, suggesting a wide range of potential diagnostic applications to detect low amounts of α2,3-sial-Gs in serum.

2. Experimental

2.1. Materials and reagents

Neu5Aca (2 − 3) GalβMP glycoside was supplied from Tokyo Chemical Industry (Japan, www.TCIchemicals.com, 90.0%). Maackia amurensis lectin (MAL) was taked from Vector Labs (USA, www.vectorlabs.com). 4-Mercaptophenylboronic acid (4-MPBA), gold (III) chloride trihydrate ($HAuCl_4{\cdot}4H_2O$), methylene blue (MB), potassium tetrachloroplatinate (II) (K_2PtCl_4) and sodium tetrachloropalladate (II) (Na_2PdCl_4) were acquired from Sigma-Aldrich (St. Louis, USA, www.sigmaadrich.com). Amino-functionalized C_{60} (n-C_{60}) was acquired from the Nanjing XFNANO Materials Tech Co., Ltd. (Nanjing, China). Phosphate-buffered solution (PBS) was prepared with KH_2PO_4 and Na_2HPO_4 containing 0.15 M NaCl (pH = 7.4). Ascorbic acid (AA), dopamine (DA), L-cysteine (L-Cys) and bovine serum albumin (BSA) were purchased from Aladdin (Shanghai, China, www.aladdin-e.com). The other chemical agents were of analytical grade and used without further purification. All aqueous solutions used Ultra-pure grade water afforded by a Millipore Milli-Q system (> 18.2 MΩ cm, USA, www.millipore.com).

2.2. Apparatus and measurements

In the electrochemical experiments, a CHI660E electrochemical workstation and a three-electrode system (Chenhua Instruments Co., Shanghai, China, instrument.cn.gongchang.com) consisting of a glassy carbon electrode (GCE, 4 mm in diameter) as the working electrode, a saturated calomel electrode (SCE) serving as the reference electrode, and a platinum electrode working as the counter electrode were used. Transmission electron microscopy (TEM) (Hitachi-7500158, Hitachi Limited, Japan, www.hitachi.com) was applied for the characterization of the nanomaterials. Field emission scanning electron microscopy (FE-SEM) images were obtained using a JEOL JSM-6700F microscope (Japan, www.jeol.co.jp). Atomic force microscopy (AFM) images were acquired with a Bruker Dimension Icon microscope (Germany, www.bruker.com). The morphologies of the materials were characterized using X-ray diffraction (XRD, Y-2000, Dandong oron ray instrument co., Ltd, China). Energy dispersive spectroscopy (EDS) measurements were performed with a JEOL JSM-6700F microscope (Japan, www.jeol.co.jp). Fourier transform infrared (FT-IR) spectra were acquired with a Nicolet 6700 FT-IR spectrometer (Thermo Nicolet, USA, www.thermofisher.com). A UV-2450 spectrophotometer (Japan, www.shimadzu.com.cn) was employed to obtain the UV–vis absorption spectra of the nanomaterials. Electrochemical impedance spectroscopy (EIS) was measured in a frequency range from 1 to 10^5 Hz. Cyclic voltammetry (CV) measurements were tested at scanning potentials between −0.2 to +0.6 V with a scan rate of 50 mV s^{-1}. X-ray photoelectron spectroscopy (XPS), with an Al Kα X-ray (1486.6 eV) light source, was performed using a VG Scientific ESCALAB 250 spectrometer (Thermoelectricity Instruments, USA). Zeta potential measurements were performed with a Zetasizer Nano ZS (ZEN3600, Malvern Instruments Ltd, UK). Differential pulse voltammetry (DPV) measurements were performed at scan potentials −0.5 to −0.1 V with a scan rate of 50 mV s^{-1} and a pulse height of 50 mV.

2.3. Preparation of n-C_{60}-PdPt

The n-C_{60}-PdPt nanocomposite was prepared on the basis of a previously reported procedure with a slight alteration (Chen et al., 2016). First, 2 mg of n-C_{60} was dispersed in 1 mL of 0.1 M HCl and then sonicated for 2 h until the n-C_{60} was symmetrically dispersed in the solution. Next, 2 mL of ultrapure water was added into the solution. Then, the mixture was heated to 100 °C. After that, 150 mg of AA, 1.17 mg of K_2PtCl_4 and 1.66 mg of Na_2PdCl_4 were added to 1 mL of ultrapure water, respectively. After heating for 2.5 h at 100 °C, the products were cooled to room temperature. Then, the mixture was centrifuged at 8000 rpm min^{-1} for 3 min and washed three times to shed the remaining AA as well as free Pt and Pd nanoparticles. In the end, the precipitate was dissolved in 1 mL of ultrapure water prior to use.

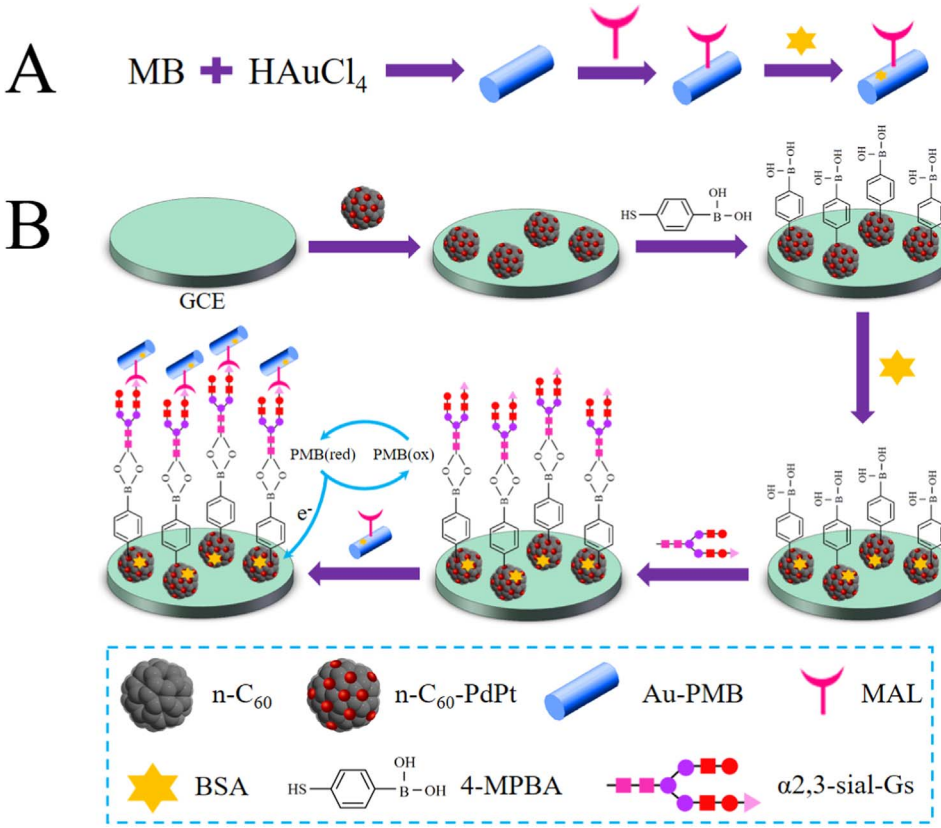

Scheme 1. (A) Schematic representation of Au-PMB-MAL; (B) Fabrication of the electrochemical biosensor.

2.4. Preparation of Au-PMB composites

The Au-PMB composites were prepared on the basis of a previously reported procedure with a slight alteration (Shan et al., 2016). The Au-PMB composites were compounded by adding HCl (0.1 M, 600 μL) and DTAB (1.14 mM, 6 mL) to MB (9.8 mM, 1 mL), and then, micelles were shaped after energetically stirring for about ten minutes. Then, $HAuCl_4$ (4%, 200 μL) was added into the compound and consecutively drastic stirred for 6 h at room temperature. The compound was centrifuged at 8000 rpm min^{-1} for 5 min and washed with ultrapure water three times. Eventually, the compound was redispersed in 2 mL of ultrapure water when not in use.

2.5. Preparation of Au-PMB-MAL composites

The preparation of Au-PMB-MAL composites was shown in Scheme 1A. First, 1 mL of the Au-PMB composites and 10 μL of MAL (2 mg mL^{-1}) were lightly mixed and stirred for 12 h at 4 °C. Then, the mixture was centrifuged at 8000 rpm min^{-1} for 5 min and rinsed thoroughly three times to shed the excess MAL. The precipitate was dissolved in 1 mL of ultrapure water prior to use. Next, 500 μL of a 1 wt % BSA was added to the compound and lightly mixed for 1 h at 4 °C, and then, the mixture was centrifuged at 8000 rpm min^{-1} for 5 min and rinsed thoroughly three times to eliminate the excess BSA. Finally, the compound was redispersed in 2 mL of ultrapure water when not in use.

2.6. Fabrication of the biosensor

The preparation process of the biosensor is exhibited in Scheme 1B. To achieve a mirror-like surface, the GCE was polished repeatedly with 0.3 and 0.05 μm alumina slurries, followed by a thorough rinsing with ultrapure water. Then, 8 μL of the prepared n-C_{60}-PdPt compound was placed onto the electrode surface and dried at room temperature. Next, 10 μL of the 4-MPBA solution was coated onto the n-C_{60}-PdPt/GCE and incubated for 12 h at 4 °C. After thorough cleaning with ultrapure water, 10 μL of a 1 wt% BSA was dropped onto the electrode surface for 30 min to prevent non-specific binding sites. After washing with water, standard α2,3-sial-Gs solutions of different concentrations were incubated onto the electrode surface for 2 h at 4 °C. Finally, 10 μL of the pre-treated Au-PMB-MAL composite was placed onto the modified electrode and incubated for 2 h at 4 °C. DPV measurements were performed at scan potentials −0.5 to −0.1 V in PBS. The generation of signals is shown in the supplementary information (S3) and Fig. S7.

3. Results and discussion

3.1. Characterization of prepared materials

The prepared materials were characterized by FE-SEM, TEM, UV–vis, FTIR, XRD, EDS and XPS (Fig. 1). Fig. 1A exhibits the FE-SEM image of n-C_{60}, which had a monodispersed spherical shape with a diameter of 100 nm. As shown in Fig. 1B, an overview FE-SEM image shows the PdPt alloy with a uniform shape coating the n-C_{60}, which manifested that the PdPt alloy was efficiently and successfully attached to n-C_{60}. Furthermore, Pd and Pt elements were displayed in the EDS of n-C_{60}-PdPt (Fig. 1E), which further illustrated that the PdPt alloy was attached onto the surface of n-C_{60}. Moreover, the XRD pattern was utilized to further indicate the successful synthesis of C_{60}-PdPt nanocomposites. The results are shown in the supplementary information (S1) and Fig. S1A.

The UV–vis spectra of MB and Au-PMB are shown in Fig. S5A, and two salient peaks were observed at 659 nm and 664 nm, which belong to MB. We can compare the UV–vis spectra of MB with that of Au-PMB, and the Au-PMB has an obvious peak at 550 nm due to the surface plasma resonance of gold nanoparticles (Tang et al., 2017). In addition, the zeta potentials of Au-PMB and MB are illustrated in Fig. S5C, which showed that unlike MB, the Au-PMB was positively charged on account

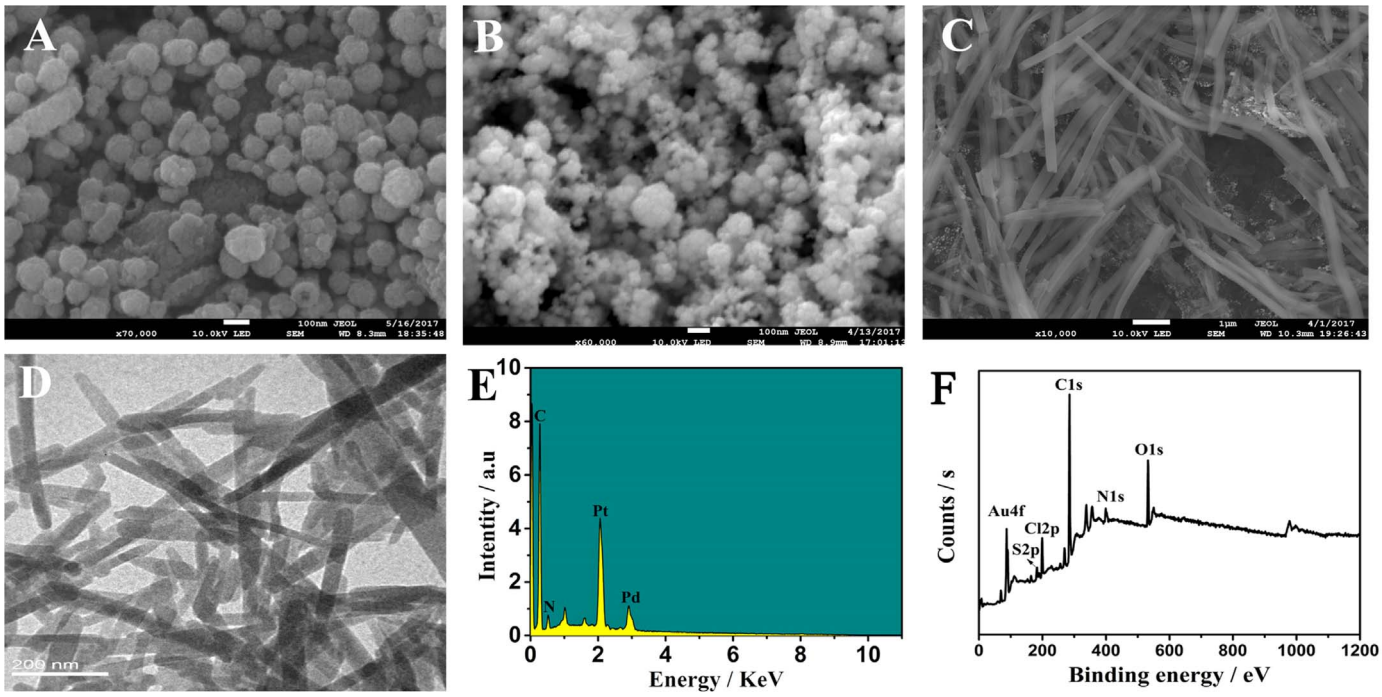

Fig. 1. FE-SEM images of (A) n-C_{60}, (B) n-C_{60}-PdPt and (C) Au-PMB; (D) TEM image of Au-PMB; (E) EDS spectrum of n-C_{60}-PdPt; (F) XPS spectrum of Au-PMB.

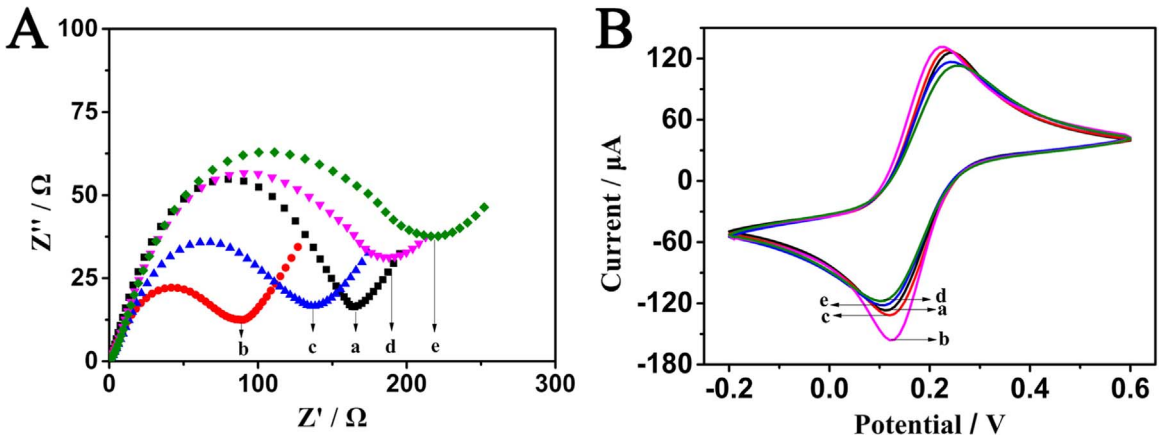

Fig. 2. Typical (A) EIS and (B) CV study in a $[Fe(CN)_6]^{3-/4-}$ (5 mM) for (a) a bare electrode, (b) n-C_{60}-PdPt/GCE, (c) 4-MPBA/n-C_{60}-PdPt/GCE, (d) blocking with 1% BSA and (e) specific recognition with 5 ng mL^{-1} α2,3-sial-Gs.

of the DTAB (Shan et al., 2016). Furthermore, Fig. S5B shows the FT-IR spectra of MB and Au-PMB, and there were the feature peak at 3000–3500 cm^{-1} that suggested a strong perturbation of the N-H stretching vibration. The band at 1599 cm^{-1} was generated by the phenyl ring vibration or a mixture of vibrations ($V_{C=N}$ and $V_{C=C}$). The characteristic peaks at 1394 cm^{-1} and 1396 cm^{-1} were demonstrated to be the vibration of C-NO_2. The peak at 885 cm^{-1} can be attributed to formed as a result of H-bonds of the type N_{het} …HO (Quintão et al., 2002). Therefore, these characteristic peaks showed the presence of MB (Ovchinnikov et al., 2016). Then, the peaks at 826 cm^{-1} were caused by the bending of the C-H bond in the phenothiazine ring (Tang et al., 2017). Since the oxidative polymerization of MB by $HAuCl_4$, previously formed the cation-radical species, $HAuCl_4$ attacked one of the methyl groups of the –$N(CH_3)_2$ moiety (Tang et al., 2017). Consequently, the FT-IR spectrum of Au-PMB exhibited the structure of MB is not destroyed and confirmed its successful synthesis. As shown in Fig. 1C and D, the ready-made Au-PMB was on the nanometre order and appeared to be stick-like nanocomposites. As shown in the EDS spectrum (Fig. S5D), typical C, N, Au, S and Cl element peaks were observed, which validated that the Au-PMB composites were successfully synthesized. Furthermore, the XPS result of Au-PMB is shown in Fig. 1F and Fig. S2. The XPS of Au-PMB shows signals for C1s at 284.98 eV, for Cl2p at 198.97 eV, for N1s at 399.31 eV, for O1s at 532.34 eV and for S2p at 164.23 eV, which belong to MB (Escard et al., 1974; Harker and Sherwood, 1973; Jin and Lin, 2004; Lin et al., 2005; Shang et al., 2008). In the Fig. 1F and Fig. S2A, the peak-to-peak distance and spectral line shape of the Au 4 f doublet were consistent with the Au° state, which were ascribed to the reduced AuNPs (Tang et al., 2017). Furthermore, the XRD pattern was utilized to prove that Au-PMB composites were successfully synthesized. The results are shown in the supplementary information (S1) and Fig. S1B.

3.2. Electrochemical characterization of the stepwise-modified electrode

To monitor the fabrication procedures of the biosensor, EIS measurements were performed in a 5 mM $[Fe(CN)_6]^{3-/4-}$ aqueous solution. The impedance spectra include a semicircle portion and a linear portion. The semicircle portion at higher frequencies represents the

electron transfer-limited process, and the linear portion at lower frequencies corresponds to the diffusion-limited process. The semicircle diameter equals the electron transfer resistance. As shown in Fig. 2A, the bare GCE revealed a small semicircle at high frequency (curve a). After the electrode was modified with n-C_{60}-PdPt, the resistance was much less than that of the bare GCE (curve b). This demonstrated that n-C_{60}-PdPt possessed a preeminent electron transfer ability at interfaces between the electrode surface and the electrolyte solution. The resistance increased after incubation with 4-MPBA (curve c), validating that 4-MPBA was linked with n-C_{60}-PdPt. On account of that the 4-MPBA is a compound with a mercapto group, the mercapto group can combine with a great number of the PdPt alloy particles (Zhang et al., 2004). A larger semicircle diameter of curve d was later found, indicating that the prepared biosensor was blocked with BSA because BSA hindered electron transfer. Afterwards, the resistance of curve e increased, confirming the successful capture of α2,3-sial-Gs, and a complex layer blocking electron transfer was generated. As shown in Fig. 2B, the pattern data are consistent with the result obtained from EIS, demonstrating the successful fabrication of the biosensor.

To monitor the fabrication procedures of the biosensor, cyclic voltammetry (CV) measurements were performed in a 5 mM $[Fe(CN)_6]^{3-/4-}$ aqueous solution. As shown in Fig. 2B, the bare GCE revealed a pair of redox peaks (curve a). After the electrode was modified with n-C_{60}-PdPt, the oxidation and reduction peak currents increased significantly (curve b). This demonstrated that n-C_{60}-PdPt possessed a preeminent electron transfer ability at interfaces between the electrode surface and the electrolyte solution. The oxidation and reduction peak currents drastic decrease after incubation with 4-MPBA (curve c), validating that 4-MPBA was linked with n-C_{60}-PdPt. Since the nonconducting 4-MPBA has the mercapto group that can combine with PdPt alloy through strong adsorption. The peak current of curve d apparently decreased, indicating that the prepared biosensor was blocked with BSA, because BSA as a blocking agent hindered electron transfer. Afterwards, the peak current curve e decreased, confirming the successful capture of α2,3-sial-Gs and that a complex layer blocking electron transfer was generated. As shown in Fig. 2B, the pattern data are consistent with the result obtained from EIS, demonstrating the successful fabrication of the biosensor.

Meanwhile, AFM is another valuable approach to characterize the fabrication of the electrode. As shown in Fig. S6, after the 4-MPBA solution was coated onto the n-C_{60}-PdPt/GCE (Fig. S6B), the surface becomes smooth compared with the n-C_{60}-PdPt modified electrode (Fig. S6A). Then, when the electrode was blocked by BSA, the surface smoothness increased a little (Fig. S6C). After α2,3-sial-Gs was coated onto the electrode, the surface became smoother due to the α2,3-sial-Gs covering the gaps in the electrode surface (Fig. S6D). All of these results further validated the successful fabrication of the proposed biosensor.

3.3. Optimization of the experimental conditions

The electrochemical performance of the biosensor is likely influenced by many parameters, such as the volume of n-C_{60}-PbPt, incubation time of 4-MPBA, concentration of 4-MPBA, and incubation time of α2,3-sial-Gs. The DPV results were acquired at a 15 Hz frequency, 25 mV pulse amplitude and voltage range of −0.1–0.5 V. The volume of the nanocomposite was investigated to further enhance the sensitivity and stability of the biosensor and to provide a favourable platform for integrating 4-MPBA. The volume of n-C_{60}-PdPt was tested in the range of 4 −12 μL. The results shown in Fig. 3A confirmed that the changes in current increased until a volume of 8 μL, and then, they remained stable. Hence, the optimal formation volume of n-C_{60}-PdPt was determined to be 8 μL.

For the recognition of α2,3-sial-Gs, the incubation time was an extremely important element. A period of time is required for the 4-MPBA to bind the glycoside and form a complex. To study the effect of the incubation time on the response signal, the fabricated biosensors were incubated for 8–16 h at 4 °C. The results in Fig. 3B exhibited that when the incubation time was longer than 12 h, the changes in current were stable, suggesting that the amount of 4-MPBA captured on the surface of the sensor reached a maximum. Therefore, 12 h was selected as the optimal incubation time.

The concentration of 4-MPBA was a notably important parameter for biosensor fabrication and may influence its sensitivity as well as stability. Fig. 3C validated that as the concentration of 4-MPBA increased from 0.1 to 1.0 mM, the peak current increased, and the current remained stable after 1.0 mM. As a consequence, a concentration of 1.0 mM of 4-MPBA was used in the further experiments.

For the recognition of α2,3-sial-Gs, the incubation time is an extremely important parameter. It requires some time to construct a novel molecular recognition system by the coordination of an amide group of Neu5Ac to the boron atom of 4-MPBA. To study the effect of the incubation time on the response signal, the fabricated biosensor was incubated with the α2,3-sial-Gs for 0.5–3 h at 4 °C. As shown in Fig. 3D, when the incubation time was longer than 2 h, the current changes remained equable. Therefore, 2 h was selected as the optimal incubation time for the experiment.

3.4. Analysis and detection

Under the optimal experimental conditions, the calibration plot for the detection of α2,3-sial-Gs was evaluated by investigating different concentrations of α2,3-sial-Gs solutions (Fig. 4A). The current signal of the proposed biosensor increased when the concentration of α2,3-sial-Gs increased, and this phenomenon indicated that the change of the current response is related to the quantity of glycoside captured on the electrode surface. The calibration plot exhibited a good linear relationship in the range of 10 fg mL^{-1} to 100 ng mL^{-1}, with the limit of detection reaching 3 fg mL^{-1} (based on S/N = 3). The linear regression equation was Y = 1.9999*logC + 6.4832, with a correlation coefficient of 0.9971 (Fig. 4B). The detection limit and linear range of the fabricated biosensor were contrasted compared with those of a prior reported biosensor for α2,3-sial-Gs in Table S1 and S3, and the fabricated biosensor had a wider range of detection.

3.5. Selectivity, stability and reproducibility of the electrochemical biosensor

To investigate the selectivity of the proposed electrochemical biosensor, we compared the effects of other endogenous molecules on the system, such as Neu5Ac α(2−6)Gal β MP glycoside (α2,6-sial-Gs) (1 μg mL^{-1}), AA (1 μg mL^{-1}), DA (1 μg mL^{-1}), glucose (1 μg mL^{-1}), L-Cys (1 μg mL^{-1}), and BSA (1 μg mL^{-1}). These experiments validated that the change in current only resulted from the specific recognition between α2,3-sial-Gs and MAL. The change in current aroused by interfering substances was less than that without these compounds (Fig. 5A), demonstrating that the selectivity of the sandwich-type biosensor was acceptable.

To investigate the stability of the biosensor, a series of biosensors were fabricated at the same time and then stored at 4 °C. After 28 days, the current responses of these biosensors remained at 89.63% of the initial current response. The results confirmed that the fabricated biosensor displayed acceptable stability. The reproducibility of the biosensor was evaluated via testing DPV signals in a 5 mL of PBS (0.1 M, pH = 7.4) with five prepared biosensors. The relative standard deviation (RSD) was 1.52% at the α2,3-sial-Gs concentration of 5 pg mL^{-1}. The results validated that this fabricated sensor also had acceptable reproducibility (Fig. 5B).

3.6. Application for the analysis of serum simples

In order to further examine the performance of the fabricated biosensor for α2,3-sial-Gs analysis in real samples. The diluted healthy human serum samples spiked with 0.1 ng mL^{-1}, 10 ng mL^{-1} and

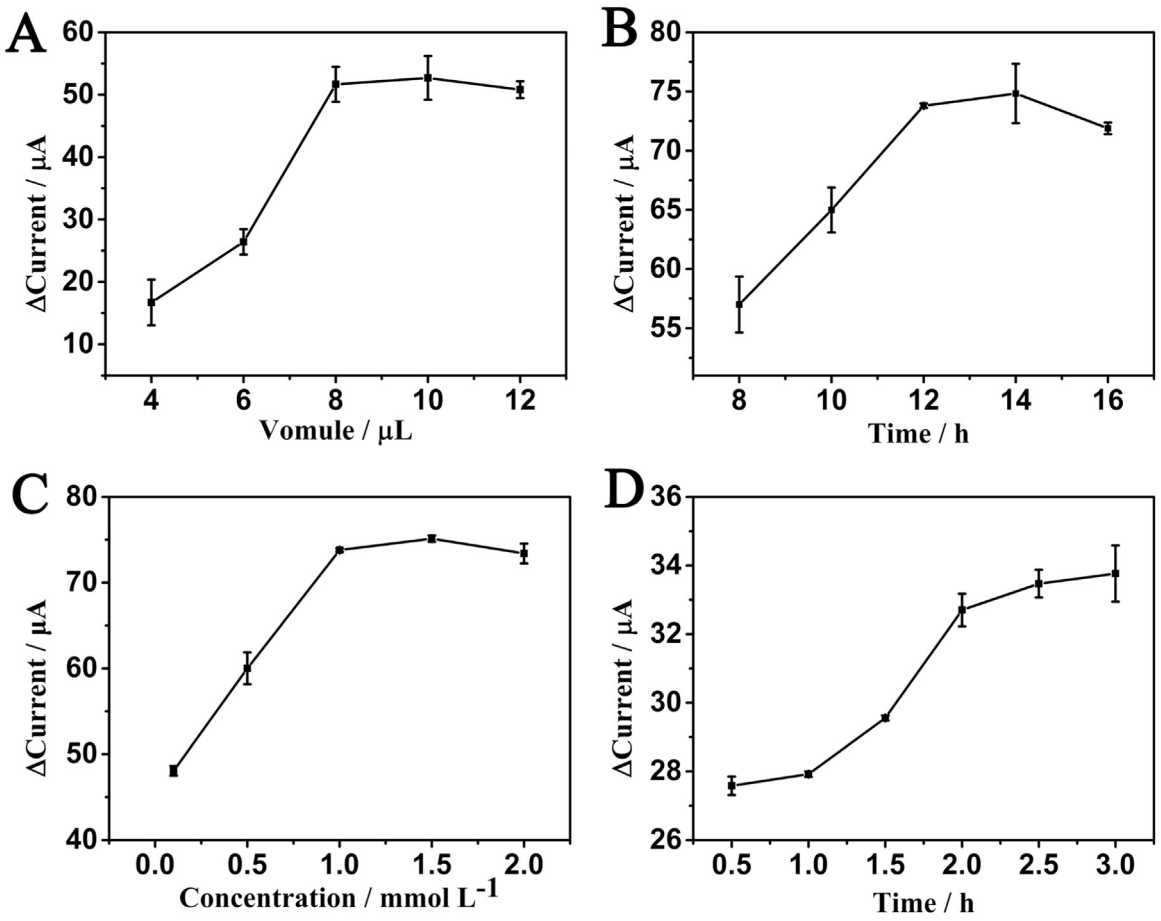

Fig. 3. Effects of the (A) volume of n-C_{60}-PdPt, (B) incubation time of 4-MPBA, (C) concentration of 4-MPBA, and (D) incubation time of α2,3-sial-Gs.

50 ng mL^{-1} of α2,3-sial-Gs were detected with the electrochemical biosensor. The detection recovery results, calculated with the averages of five replicates and shown in Table S2, were 98.72–100.41%, and the RSDs were less than 5%. The above results suggested that the proposed sensor assay can identify the α2,3-sial-Gs in human serum samples.

4. Conclusions

In this research, a specific and ultrasensitive sandwich-type electrochemical biosensor, was fabricated for the detection of α2,3-sial-Gs in human serum. We used 4-MPBA@n-C_{60}-PdPt as the sensing platform which can accelerated the electron transfer rate and improved the sensitivity of the biosensor. MAL-functionalized Au-PMB can be specifically recognized by α2,3-sial-Gs and generated an electrochemical signal. Under optimal conditions, the prepared biosensor exhibited superior analytical performance with a wide examination area, a low detection limit, good recovery and good stability. This biosensor has potential application for detecting the other glycoproteins in clinical practice. However, the preparation phase of the biosensor is time consuming. We are trying to explore a one-step polymerization of materials to reduce the consumption of time and provide tools for rapid diagnosis and clinical research.

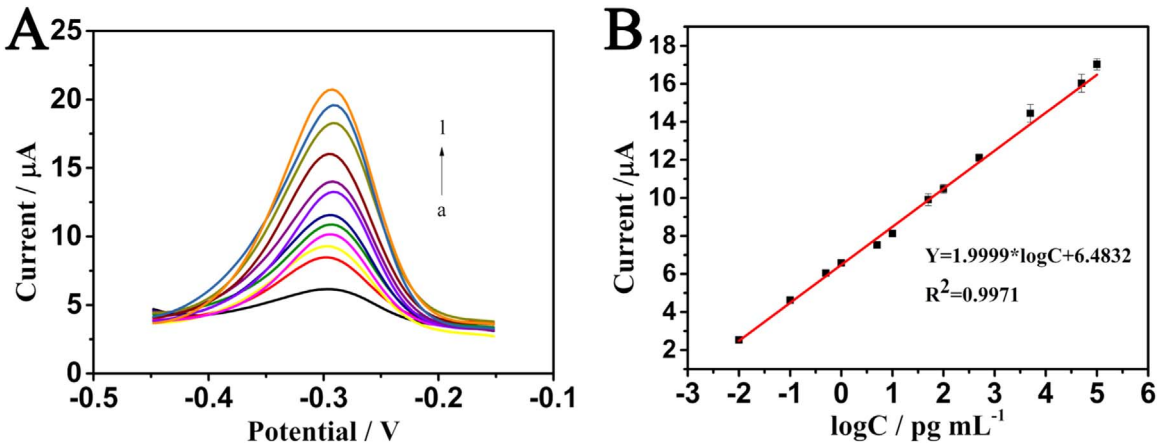

Fig. 4. (A) The DPVs of the biosensor after incubation in different concentrations of α2,3-sial-Gs, standard solution (from a to l): 10 fg mL^{-1}, 100 fg mL^{-1}, 0.5 pg mL^{-1}, 1 pg mL^{-1}, 5 pg mL^{-1}, 10 pg mL^{-1}, 100 pg mL^{-1}, 500 pg mL^{-1}, 5 ng mL^{-1}, 50 ng mL^{-1} and 100 ng mL^{-1}; (B) Calibration curve of the biosensor toward different concentrations of α2,3-sial-Gs.

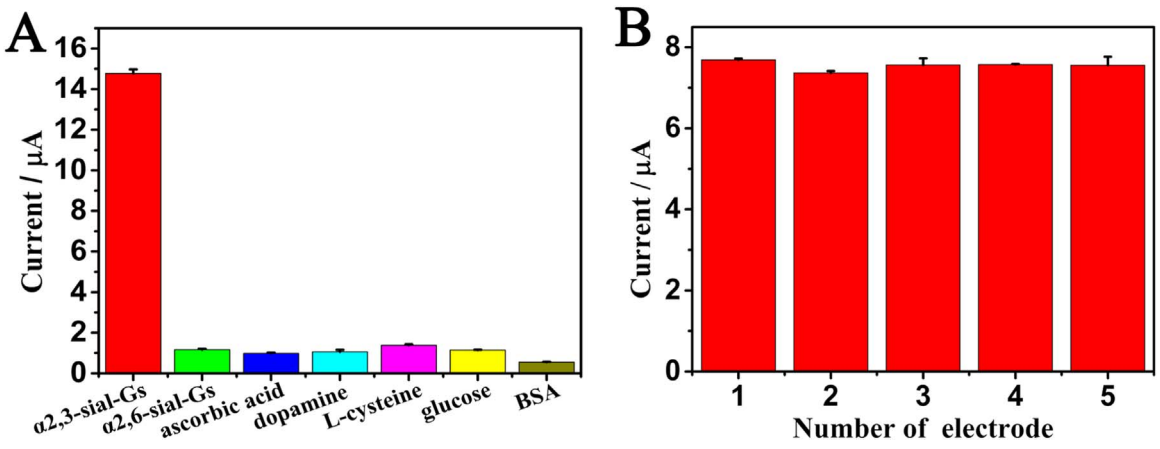

Fig. 5. Interference study (A), response of the sensor to α2,3-sial-Gs (5 ng mL^{-1}), α2,6-sial-Gs (1 μg mL^{-1}), AA (1 μg mL^{-1}), DA (1 μg mL^{-1}), glucose (1 μg mL^{-1}), L-Cys (1 μg mL^{-1}), and BSA (1 μg mL^{-1}). (B) Reproducibility of five different electrodes modified with 5 pg mL^{-1} α2,3-sial-Gs.

Acknowledgments

We are grateful for the financial support from the National Nature Science Foundation of China (No. 81370403), the Chongqing Foundation and Advanced Research Project (No. CSTC2015jcyjBX0053), the Chongqing Precision Medical Key Technology Research and Development and Demonstration Projects (cstc2016shms-ztzx0042) and the Chongqing Medical University Scientific Research Cultivating Fund (No. 201414).

Appendix A. Supporting information

Supplementary data associated with this article can be found in the online version at http://dx.doi.org/10.1016/j.bios.2017.11.043.

References

Chen, Q., Yu, C., Gao, R., Gao, L., Li, Q., Yuan, G., He, J., 2016. Biosens. Bioelectron. 79, 364–370.
Chen, X., Varki, A., 2010. ACS Chem. Biol. 5, 163–176.
Everest-Dass, A.V., Abrahams, J.L., Kolarich, D., Packer, N.H., Campbell, M.P., 2013. J. Am. Soc. Mass Spectrom. 24, 895–906.
Escard, J., Mavel, G., Guerchais, J.E., Kergoat, R., 1974. Inorg. Chem. 13, 695–701.
Feng, J., Li, Y., Li, M., Li, F., Han, J., Dong, Y., Chen, Z., Wang, P., Liu, H., Wei, Q., 2017. Biosens. Bioelectron. 91, 441–448.
Gao, L., He, J., Xu, W., Zhang, J., Hui, J., Guo, Y., Li, W., Yu, C., 2014. Biosens. Bioelectron. 62, 79–83.
Geisler, C., Jarvis, D.L., 2011. Glycobiology 21, 988–993.
Harduin-Lepers, A., Vallejo-Ruiz, V., Krzewinski-Recchi, M.-A., Samyn-Petit, B., Julien, S., Delannoy, P., 2001. Biochimie 83, 727–737.
Harker, H., Sherwood, P.M.A., 1973. Philos. Mag. 27, 1241–1244.
Hsiao, C.J., Tzai, T.S., Chen, C.H., Yang, W.H., Chen, C.H., 2016. Dis. Markers 2016, 8915809.
Jin, G.P., Lin, X.Q., 2004. Electrochem. Commun. 6, 454–460.
Kang, J., Park, H.M., Kim, Y.W., Kim, Y.H., Varghese, S., Seok, H.K., Kim, Y.G., Kim, S.H., 2014. Eur. Cells Mater. 28, 387–403.
Kavosi, B., Hallaj, R., Teymourian, H., Salimi, A., 2014. Biosens. Bioelectron. 59, 389–396.
Kim, S., Oh, D.B., Kang, H.A., Kwon, O., 2011. Appl. Microbiol. Biot. 91, 1–15.
Leppanen, A., Stowell, S., Blixt, O., Cummings, R.D., 2005. J. Biol. Chem. 280, 5549–5562.
Li, M., Bo, X., Zhang, Y., Han, C., Guo, L., 2014. Biosens. Bioelectron. 56, 223–230.
Li, Y., Fang, L., Cheng, P., Deng, J., Jiang, L., Huang, H., Zheng, J., 2013. Biosens. Bioelectron. 49, 485–491.
Lin, X.Q., Jiang, X.H., Lu, L.P., 2005. Biosens. Bioelectron. 20, 1709–1717.
Niu, Y., He, J., Li, Y., Zhao, Y., Xia, C., Yuan, G., Zhang, L., Zhang, Y., Yu, C., 2016. Microchim. Acta 183, 2337–2344.
Otsuka, H., Uchimura, E., Koshino, H., Okano, T., Kataoka, K., 2003. J. Am. Chem. Soc. 125, 3493–3502.
Ovchinnikov, O.V., Evtukhova, A.V., Kondratenko, T.S., Smirnov, M.S., Khokhlov, V.Y., Erina, O.V., 2016. Vib. Spectrosc. 86, 181–189.
Palmisano, G., Larsen, M.R., Packer, N.H., Thaysen-Andersen, M., 2013. RSC Adv. 3, 22706.
Park, J.J., Yi, J.Y., Jin, Y.B., Lee, Y.J., Lee, J.S., Lee, Y.S., Ko, Y.G., Lee, M., 2012. Biochem. Pharmacol. 83, 849–857.
Patil, S.A., Bshara, W., Morrison, C., Chandrasekaran, E.V., Matta, K.L., Neelamegham, S., 2014. Glycoconj. J. 31, 509–521.
Quintão, A.D., Coutinho, K., Canuto, S., 2002. Int. J. Quantum Chem. 90, 634–640.
Saarinen, J., Welgus, H.G., Flizar, C.A., Kalkkinen, N., Helin, J., 1999. Eur. J. Biochem. 259, 829–840.
Shan, J., Wang, L., Ma, Z., 2016. Sens. Actuators B: Chem. 237, 666–671.
Shang, N.G., Papakonstantinou, P., McMullan, M., Chu, M., Stamboulis, A., Potenza, A., Dhesi, S.S., Marchetto, H., 2008. Adv. Funct. Mater. 18, 3506–3514.
Tang, Z., Wang, L., Ma, Z., 2017. Biosens. Bioelectron. 92, 577–582.
Xia, N., Deng, D., Zhang, L., Yuan, B., Jing, M., Du, J., Liu, L., 2013. Biosens. Bioelectron. 43, 155–159.
Zhang, D.-q., Gao, L.-x., Zhou, G.-d., 2004. Corros. Sci. 46, 3031–3040.
Zhang, L., Wang, Y., Wang, J., Shi, J., Deng, K., Fu, W., 2013. Biosens. Bioelectron. 50, 217–223.